Title

Altered network connectivity in frontotemporal dementia with C9orf72 hexanucleotide repeat expansion

Journal

Brain, 137(11)

ISSN

0006-8950

Authors

Lee, Suzee E

Khazenzon, Anna M

Trujillo, Andrew J

et al.

Publication Date

2014-11-01

DOI

10.1093/brain/awu248

Peer reviewed

doi:10.1093/brain/awu248 Brain 2014: 137; 3047–3060 | 3047

BRAIN
A JOURNAL OF NEUROLOGY

Altered network connectivity in frontotemporal dementia with *C9orf72* hexanucleotide repeat expansion

Suzee E. Lee,[1] Anna M. Khazenzon,[1] Andrew J. Trujillo,[1] Christine C. Guo,[1] Jennifer S. Yokoyama,[1] Sharon J. Sha,[1] Leonel T. Takada,[2] Anna M. Karydas,[1] Nikolas R. Block,[1] Giovanni Coppola,[3] Mochtar Pribadi,[3] Daniel H. Geschwind,[3] Rosa Rademakers,[4] Jamie C. Fong,[1] Michael W. Weiner,[5] Adam L. Boxer,[1] Joel H. Kramer,[1] Howard J. Rosen,[1] Bruce L. Miller[1] and William W. Seeley[1,6]

1 Memory and Ageing Centre, Department of Neurology, University of California, San Francisco, CA 94158, USA
2 Department of Neurology, Hospital das Clínicas, University of Sao Paulo Medical School, Sao Paolo, Brazil
3 Department of Neurology and Department of Psychiatry, Semel Institute for Neuroscience and Human Behavior, University of California, Los Angeles, CA 90095, USA
4 Department of Neuroscience, Mayo Clinic Florida, Jacksonville, FL 32224, USA
5 Centre for Imaging of Neurodegenerative Diseases, Department of Veterans Affairs Medical Centre, San Francisco, CA 94121, USA and Department of Radiology, University of California, San Francisco, CA 94143, USA
6 Department of Pathology, University of California, San Francisco, CA 94143, USA

Correspondence to: Suzee E. Lee, MD,
UCSF Department of Neurology,
Memory and Ageing Centre,
675 Nelson Rising Lane,
Suite 190, MC: 1207,
San Francisco,
CA 94158, USA
E-mail: suzeelee@memory.ucsf.edu

Hexanucleotide repeat expansion in *C9orf72* represents the most common genetic cause of familial and sporadic behavioural variant frontotemporal dementia. Previous studies show that some *C9orf72* carriers with behavioural variant frontotemporal dementia exhibit distinctive atrophy patterns whereas others show mild or undetectable atrophy despite severe behavioural impairment. To explore this observation, we examined intrinsic connectivity network integrity in patients with or without the *C9orf72* expansion. We studied 28 patients with behavioural variant frontotemporal dementia, including 14 *C9orf72* mutation carriers (age 58.3 ± 7.7 years, four females) and 14 non-carriers (age 60.8 ± 6.9 years, four females), and 14 age- and sex-matched healthy controls. Both patient groups included five patients with comorbid motor neuron disease. Neuropsychological data, structural brain magnetic resonance imaging, and task-free functional magnetic resonance imaging were obtained. Voxel-based morphometry delineated atrophy patterns, and seed-based intrinsic connectivity analyses enabled group comparisons of the salience, sensorimotor, and default mode networks. Single-patient analyses were used to explore network imaging as a potential biomarker. Despite contrasting atrophy patterns in *C9orf72* carriers versus non-carriers, patient groups showed topographically similar connectivity reductions in the salience and sensorimotor networks. Patients without *C9orf72* expansions exhibited increases in default mode network connectivity compared to controls and mutation carriers. Across all patients,

Received February 28, 2014. Revised June 3, 2014. Accepted July 22, 2014. Advance Access publication October 1, 2014

behavioural symptom severity correlated with diminished salience network connectivity and heightened default mode network connectivity. In *C9orf72* carriers, salience network connectivity reduction correlated with atrophy in the left medial pulvinar thalamic nucleus, and this region further showed diminished connectivity with key salience network hubs. Single-patient analyses revealed salience network disruption and default mode network connectivity enhancement in *C9orf72* carriers with early-stage or slowly progressive symptoms. The findings suggest that patients with behavioural variant frontotemporal dementia with or without the *C9orf72* expansion show convergent large-scale network breakdowns despite distinctive atrophy patterns. Medial pulvinar degeneration may contribute to the behavioural variant frontotemporal dementia syndrome in *C9orf72* carriers by disrupting salience network connectivity. Task-free functional magnetic resonance imaging shows promise in detecting early-stage disease in *C9orf72* carriers and may provide a unifying biomarker across diverse anatomical variants.

Keywords: frontotemporal dementia; functional connectivity; dementia; biomarkers; amyotrophic lateral sclerosis

Abbreviations: ALS = amyotrophic lateral sclerosis; DMN = default mode network; FTD = frontotemporal dementia; FTDC = Frontotemporal Dementia Consortium; ICN = intrinsic connectivity network; MND = motor neuron disease; NPI = Neuropsychiatric Inventory; SMN = sensorimotor network

Introduction

Hexanucleotide expansion in *C9orf72* represents the most common genetic mutation causing familial and sporadic behavioural variant frontotemporal dementia (bvFTD) and amyotrophic lateral sclerosis (ALS) (DeJesus-Hernandez *et al*., 2011; Renton *et al*., 2011). Previous series reveal heterogeneous clinical presentations in *C9orf72* carriers, whose predominant phenotypes include bvFTD, bvFTD with motor neuron disease (bvFTD-MND), and ALS (DeJesus-Hernandez *et al*., 2011; Renton *et al*., 2011). In some bvFTD series, *C9orf72* carriers manifested greater psychosis and episodic memory impairment than non-carriers (Boeve *et al*., 2012; Simón-Sánchez *et al*., 2012; Snowden *et al*., 2012), but the core bvFTD clinical features emerge regardless of *C9orf72* status.

Group-level neuroimaging analyses demonstrate that patients with *C9orf72*+ bvFTD show symmetric atrophy most prominent in the anterior insula, anterior cingulate, and frontotemporal cortex, in keeping with the sporadic bvFTD-associated pattern (Boxer *et al*., 2011; Mahoney *et al*., 2012; Sha *et al*., 2012; Whitwell *et al*., 2012; Irwin *et al*., 2013). Some studies have reported that *C9orf72* carriers also show parietal (Sha *et al*., 2012; Whitwell *et al*., 2012; Irwin *et al*., 2013) and occipital (Sha *et al*., 2012; Whitwell *et al*., 2012) atrophy not typical of sporadic bvFTD, creating a more distributed atrophy pattern. Patient-level findings suggest even greater heterogeneity; patients with mild, slowly progressive, or even advanced dementia may show little or no atrophy (Boeve *et al*., 2012; Khan *et al*., 2012). Some group-level studies have described greater thalamic (Mahoney *et al*., 2012; Sha *et al*., 2012; Irwin *et al*., 2013) and cerebellar (Mahoney *et al*., 2012; Whitwell *et al*., 2012; Irwin *et al*., 2013) atrophy in *C9orf72*+ bvFTD, whereas others have emphasized mild atrophy in frontal, temporal, insular and parietal cortex with no significant thalamic atrophy (Whitwell *et al*., 2012).

We reasoned that intrinsic connectivity network (ICN) analysis could help clarify systems-level dysfunction in *C9orf72*+ bvFTD, including patients with atypical, mild, or absent structural brain atrophy. ICNs are temporally synchronous, low frequency (<0.08 Hz) fluctuations in blood oxygen level-dependent signal and correspond with regional ensembles recruited in task-activation functional MRI studies (Smith *et al*., 2009). Neurodegenerative disease syndromes have been linked to atrophy within distinct ICNs (Seeley *et al*., 2009), and ICN measures have proven sensitive to disease even in regions lacking structural atrophy (Gardner *et al*., 2013; Dopper *et al*., 2014). Previous studies have identified bvFTD-associated atrophy (Seeley *et al*., 2009) and intrinsic connectivity disruptions (Zhou *et al*., 2010; Whitwell *et al*., 2011; Farb *et al*., 2013; Filippi *et al*., 2013) in the salience network, an ICN whose major nodes include the anterior insula, anterior cingulate cortex, amygdala, ventral striatum, and medial thalamus, regions proposed to represent the emotional significance of internal and external stimuli and coordinate contextualized viscero-autonomic, cognitive, and behavioural responses (Seeley *et al*., 2007). While the anterior 'social brain' degenerates in bvFTD, posterior cortical functions may flourish, corresponding with focally enhanced intrinsic connectivity within a hippocampal-cingulo-temporal-parietal network referred to as the default mode network (DMN) (Zhou *et al*., 2010; Borroni *et al*., 2012; Whitwell *et al*., 2011; Farb *et al*., 2013). In ALS, studies of a sensorimotor network (SMN) composed of primary motor and sensory cortices and supplementary motor areas (Biswal *et al*., 1995) show connectivity decreases in dorsomedial prefrontal cortex (Mohammadi *et al*., 2009) and primary motor cortex (Tedeschi *et al*., 2012), and increases in Rolandic, premotor, and dorsolateral prefrontal cortices (Douaud *et al*., 2011), suggesting unbalanced or compensatory network connectivity.

Here, we compared intrinsic connectivity in 14 patients with *C9orf72*+ bvFTD (five with comorbid MND) with 14 patients with sporadic bvFTD (five with MND) and healthy control participants. We hypothesized that (i) patients with bvFTD with or without *C9orf72* expansions would demonstrate convergent salience network connectivity reductions, reflecting the shared bvFTD syndrome; (ii) bidirectional SMN connectivity changes consistent with the ALS literature would be seen in both patient groups, each including five patients with MND; and (iii) *C9orf72*+ bvFTD would exhibit greater DMN connectivity reduction compared with sporadic bvFTD, in line with previous studies reporting greater parietal atrophy in *C9orf72*+ bvFTD. We also explored

connectivity-behaviour correlations and single-patient ICN analyses in early-stage and slowly progressive disease.

Materials and methods

Participants

Fourteen right-handed *C9orf72* carriers (negative for *MAPT* and *GRN* mutations) in the University of California, San Francisco Memory and Aging Centre database met bvFTD criteria (Neary *et al*., 1998) and had undergone task-free functional MRI scanning. Patients were diagnosed prospectively with consensus criteria in use at the time of evaluation (Neary *et al*., 1998) and reassessed using the Frontotemporal Dementia Consortium (FTDC) criteria (Rascovsky *et al*., 2011). Twelve of 14 met probable and two met possible bvFTD FTDC criteria due to a lack of brain imaging abnormalities. Five of 14 patients with *C9orf72*+ bvFTD had comorbid MND. Patients were designated bvFTD-MND if they met Neary bvFTD criteria and (i) probable ALS criteria (Brooks *et al*., 2000); or (ii) had evidence of ALS-spectrum disease (primary lateral sclerosis or lower motor neuron signs) involving bulbar musculature or more than one spinal level. A bvFTD comparison group, negative for *MAPT*, *GRN*, and *C9orf72* mutations (Supplementary material) was matched to the *C9orf72*+ bvFTD patients for age, sex, education, handedness and scanner. All *C9orf72*− bvFTD patients met Neary and probable bvFTD FTDC criteria. In each bvFTD group, four patients had bvFTD-ALS and one had bvFTD-MND (with predominant upper motor neuron involvement). The proportion taking CNS-acting medications did not differ among patients with or without *C9orf72* ($\chi^2 = 2.8$, $P = 0.09$; Supplementary material).

Neurological and neuropsychological assessments occurred within 180 days of MRI scanning. The Frontotemporal Lobar Degeneration-modified Clinical Dementia Rating (FTLD-CDR) scale evaluated functional status (Morris, 1993; Knopman *et al*., 2008). The Neuropsychiatric Inventory (NPI) measured behavioural symptoms (Cummings *et al*., 1994); we created an NPI composite score, the sum of the apathy, disinhibition, eating, euphoria, and aberrant motor behaviour subscales, because four of these subscales (apathy, disinhibition, eating, and aberrant motor behavior) parallel the FTDC core bvFTD clinical criteria, and all five (including euphoria) are significantly increased in patients with FTD compared with Alzheimer's disease (Liu *et al*., 2004).

Healthy controls for voxel-based morphometry (HC1, $n = 42$, Supplementary material) and task-free functional MRI (HC2, $n = 14$) were matched to patient groups for age, sex, education, handedness and scanner. All HC2 had a FTLD-CDR = 0 and those tested ($n = 10$) had a Mini-Mental State Examination score (Folstein *et al*., 1983) >27/30; both HC1 and HC2 had no significant history of neurological disease, and a brain MRI free of significant white matter changes or other lesions.

We performed single-patient voxel-based morphometry and task-free functional MRI analyses on four *C9orf72* carriers. Two had mild behavioural symptoms not meeting Neary or FTDC bvFTD criteria, and two previously described carriers included in the group analyses had slowly progressive bvFTD (Khan *et al*., 2012). For single patient analyses, 30 healthy control participants were matched to each patient for age, sex, education, handedness, and scanner (Supplementary material). Patient anonymity was protected by altering minor clinical details.

The University of California, San Francisco Committee on Human Research approved the study. Participants or their surrogates provided informed consent before participation.

Image acquisition

Ten participants per patient group underwent 3 T MRI scanning; four per patient group underwent 4 T MRI scanning. Healthy controls for voxel-based morphometry and ICN analyses were scanned at an equal proportion of 3 T and 4 T scans as the patient groups (Supplementary material).

Structural imaging

Volumetric magnetization prepared rapid gradient echo sequences obtained T_1-weighted images with parameters as follows: 3 T: repetition time: 2300 ms; echo time: 2.98 ms; flip angle 9°; 160 sagittal slices; matrix size 240 × 256; voxel size = 1 mm^3; and 4 T: 2300 ms; echo time: 3.37 ms; flip angle 7°; 176 sagittal slices; matrix size 256 × 256; voxel size = 1 mm^3.

Functional imaging

The 3 T scanner acquired 240 functional MRI images comprised of 36 interleaved axial slices (3 mm thick, 0.6 mm gap) using a T_2*-weighted echo-planar imaging sequence (repetition time: 2000 ms; echo time: 27 ms; flip angle: 80°; field of view: 230 mm^2; matrix size: 92 × 92; in-plane voxel size: 2.5 mm^2) with an online gradient adjustment for head motion compensation. The 4 T scanner functional MRI images consisted of 32 interleaved axial slices (3.5 mm thick) using a T_2*-weighted gradient echo spiral pulse sequence (repetition time: 2500 ms; echo time: 30 ms; flip angle: 90°; field of view: 225 mm^2; matrix size: 64 × 64; isotropic in-plane spatial resolution 3.52 mm). Because the number of volumes acquired by the 4 T scanner ranged from 144 to 180, all scans were truncated to 144 images. Before scanning, participants were instructed to remain awake with their eyes closed.

To minimize confounding effects of using two scanners, we balanced patient and control groups for scanner site and entered site as a nuisance covariate in all regression analyses, following previous approaches (Zhou *et al*., 2010; Sha *et al*., 2012).

Image processing and analysis

Structural imaging

Voxel-based morphometry was performed using the SPM8 VBM8 toolbox (http://www.fil.ion.ucl.ac.uk/spm/). T_1-weighted images were preprocessed with VBM8 default estimation settings, normalized using standard spatial normalization with a light clean up, modulated, corrected for non-linear warping, then segmented into grey and white matter images. Grey matter images were smoothed using an 8 mm full-width at half-maximum isotropic Gaussian kernel. As our primary question concerned how patients with bvFTD with and without the *C9orf72* expansion differ from control participants (HC) and from each other, we used two-sample *t*-tests to compare smoothed grey matter maps between: (i) *C9orf72*+ < HC1; (ii) *C9orf72*− < HC1; (iii) *C9orf72*+ < *C9orf72*−; (iv) *C9orf72*+ > *C9orf72*−. Nuisance covariates included age, sex, scanner, and total intracranial volume.

Although *C9orf72*+ and *C9orf72*− bvFTD showed no significant differences on the FTLD-CDR sum of boxes score (FTLD-CDR-SB), we chose to adjust for the potential influence of clinical severity on neuroimaging results by including FTLD-CDR-SB as a nuisance covariate.

For single-patient voxel-based morphometry, we compared each patient's smoothed grey matter image with a matched control group, following previous approaches (Khan *et al*., 2012).

Functional imaging

Preprocessing: We discarded initial functional images to allow for magnetic field stabilization (3 T scanner = 5, 4 T scanner = 6 volumes). Functional images were spatially realigned, unwarped, and slice-time corrected. Unwarping was performed to reduce artefacts due to movement-by-deformation interactions. Co-registration was performed between the mean T_2* images and the participant's own T_1-weighted image, and statistical parametric mapping (SPM) non-linear normalization was carried out by calculating the warping parameters between the participant's T_1-weighted image and the Montreal Neurological Institute T_1 template and applying the parameters to all functional images in the sequence. Subsequently, functional images were resampled at a voxel size of $2\,mm^3$. Functional images were smoothed with a 4 mm full-width at half-maximum Gaussian kernel.

Head motion: We used the SPM8 realign algorithm to determine participants' head motion using rigid body parameters. No patient required exclusion for exceeding our threshold of $\geqslant 3$ mm translational movement between functional MRI volumes. We computed mean root-mean-square values of volume-to-volume changes in translational (in mm) and rotational (mean Euler angle) movement because these metrics correlate with network connectivity strength (Van Dijk *et al*., 2012). Two-sample *t*-tests revealed a small but statistically significant difference between all patients' and controls' mean root-mean-square values for translational (0.2 ± 0.1 mm versus 0.1 ± 0.1 mm, respectively, $P < 0.01$) but not rotational (0.003 ± 0.002 radians versus 0.002 ± 0.001 radians, respectively, $P = 0.06$) movement. Rather than excluding participants from the small *C9orf72+* group, we used the Artifact Detection Tools toolbox (http://www.nitrc.org/projects/artifact_detect/) to reduce the impact of group differences in motion (Ofen *et al*., 2007). Images were identified as outliers if (i) movement from the preceding image exceeded 1 mm (defined by a composite motion score representing the Euclidean sum of three translational and three rotational directions); or (ii) the global mean intensity of the image was greater than three standard deviations from the functional MRI acquisition's mean image. Nuisance covariates in the subject-level regression model included the composite motion score, six motion parameters, and the outlier volumes.

Region of interest analyses: Seed regions of interest were used to derive three ICNs: (i) salience network: right ventral anterior insula (i.e. fronto-insula) (Seeley *et al*., 2008); (ii) SMN: right precentral gyrus (Zielinski *et al*., 2010); and (iii) DMN: right angular gyrus (Seeley *et al*., 2009). Seeds consisted of 4 mm radius spheres centred at the chosen coordinates (Supplementary material). Using the MARSBAR toolbox for SPM8 (Brett *et al*., 2002), we extracted the average blood oxygen level-dependent signal intensity of all voxels within a given seed for each volume throughout each participant's scan. Resulting region of interest time series served as covariates of interest for whole-brain regression analyses, resulting in three ICN maps for each participant. To reduce effects of physiological noise, we included masks of the CSF, white matter, and non-brain regions as nuisance covariates in the subject-level regression model. Two sample *t*-tests compared ICN maps for: (i) *C9orf72+* versus HC2; (ii) *C9orf72−* versus HC2; and (iii) *C9orf72+* versus *C9orf72−*. We regressed FTLD-CDR-SB as a nuisance covariate for patient group contrasts. Using the Biological Parametric Mapping toolbox (Casanova *et al*., 2007), we entered each participant's voxel-based morphometry grey matter map as a set of voxelwise covariates to assess potential effects of atrophy on ICN strength. To evaluate the impact of 'high motion' participants on our major findings, we repeated group ICN analyses after excluding the two *C9orf72+* and two *C9orf72−* patients with the highest mean root-mean-square values (Supplementary material).

For single-patient functional MRI analyses, we compared each patient's ICN correlation maps with a matched control group ($n = 30$) using a statistical approach similar to previous single-patient VBM analyses (Khan *et al*., 2012).

We masked all group and single patient statistical maps to the relevant ICN. ICN masks were derived from 15 independent healthy control participants using independent component analysis (Habas *et al*., 2009) and included subcortical regions and the cerebellum, regions often omitted in independent component analysis-based network renderings (Zhou *et al*., 2012).

Correlations between network connectivity and clinical severity: We correlated patients' NPI composite scores with their single-subject ICN maps to yield a single map per network showing regions significantly correlated with the NPI composite.

Interaction of C9orf72 status with grey matter/network connectivity correlations with NPI: We performed a voxelwise analysis seeking regions in which *C9orf72+* and *C9orf72−* showed a differing correlation slope for the relationship between NPI and grey matter atrophy or NPI and ICN connectivity using multiple regression in SPM8.

Correlation between salience network connectivity and thalamic grey matter atrophy: We calculated a salience network mean connectivity score for each *C9orf72+* patient by calculating the mean beta value across all voxels within a map of regions showing salience network reduction in *C9orf72+* bvFTD versus controls, defined using a less stringent joint cluster and extent threshold ($P < 0.1$) to capture a broader landscape of connectivity reductions. We first correlated the salience network mean connectivity score with grey matter intensity across the entire brain and then restricted the analysis to the bilateral thalamus. We repeated this mean salience network connectivity correlation with the entire brain and the bilateral thalamus for *C9orf72−* bvFTD. We then conducted a seed-based ICN analysis using the thalamic cluster in which grey matter atrophy correlated with salience network connectivity reductions in *C9orf72+* bvFTD.

Statistical thresholding for neuroimaging analyses

Voxel-based morphometry: For patient versus control comparisons, grey matter/network connectivity correlations with NPI, and single-patient analyses, significant clusters were defined using a *t*-threshold corresponding to $P < 0.05$ family-wise error corrected. For contrasts between patient groups, we set a *t*-threshold corresponding to $P < 0.001$ (uncorrected). For correlations between salience network connectivity and grey matter atrophy, we identified significant clusters at $P < 0.01$ uncorrected. Clusters contained a minimum of 50 voxels.

Task-free functional MRI: For group-level and single-patient analyses and correlations between network connectivity and clinical severity, we used joint probability distribution thresholding (Poline *et al*., 1997) with a joint height and extent threshold of $P < 0.05$ corrected at the whole-brain level. Binary ICN masks used for visualizing in-network findings were created by tailoring the statistical threshold to generously constrain the search volume for the ICN contrasts at a *t*-score $\geqslant 2.5$ (Habas *et al*., 2009).

Statistical analyses

We compared clinical and neuroimaging variables using *t*-test, ANOVA, Kruskal-Wallis or Mann-Whitney U, as appropriate. Test statistics were considered significant at $P < 0.05$ (two-tailed).

Table 1 Participants' demographic and neuropsychological features

	Healthy controls	*C9orf72* carriers	Non-carriers	Test statistic, df	*P*
bvFTD: bvFTD-MND, *n*	NA	9:5	9:5	NA	
Age at MRI scan, years	62.2 (4.7)	58.3 (7.7)	60.8 (6.9)	$F = 1.3, 41$	0.29
M:F, *n*	10:4	10:4	10:4	NA	
Education, years	15.9 (2.0)	14.9 (3.7)	16.4 (2.3)	$F = 1.1, 41$	0.36
Age at symptom onset, years	NA	50.6 (12.6)	55.7 (7.2)	$t = -1.3, 26$	0.20
Disease duration, years	NA	7.8 (7.9)	5.1 (2.8)	U = 87, NA	0.64
Modified Goldman score (median, range)	NA	1.5 (1.0–4.0)	3.5 (2.0–4.0)	NA	
FTLD-CDR, total (median, range)	0 (0)	1.0 (0.5–2.0)	1.0 (0.5–3.0)	NA	
FTLD-CDR, sum of boxes	0 (0)	6.6 (3.1)	7.1 (3.1)	$t = -0.5, 26$	0.65
Mini-Mental State Exam (max = 30)	29.6 (0.7)$^{+,-}$	25.2 (3.5)	25.8 (3.9)	K = 16.5, 2	<0.01
California Verbal Learning Test, short form, four learning trials, total (max = 36)	NC	20.1 (6.6)	18.5 (7.1)	$t = 0.5, 20$	0.60
California Verbal Learning Test, Short Form, 10 min recall, score (max = 9)	NC	5.3 (2.6)	3.9 (2.7)	$t = 1.2, 20$	0.25
Benson figure copy (max = 17)	15.2 (1.3)	13.7 (2.9)	14.0 (2.0)	K = 2.1, 2	0.35
Benson figure 10 min recall (max = 17)	12.2 (1.6)	9.3 (6.5)	7.4 (4.9)	K = 4.4, 2	0.11
Digit span backward	5.3 (1.3)$^{+}$	3.3 (1.4)	3.8 (1.3)	K = 9.5, 2	<0.01
Modified trails (correct lines per min)	29.9 (9.9)$^{-}$	21.0 (11.4)	11.4 (10.5)	$F = 7.3, 26$	<0.01
Modified trails errors (median, range)	1.0 (0–2.0)	2.0 (0–6.0)	0 (0–2.0)	NA	
Design fluency (correct designs per min)	10.0 (2.1)$^{+,-}$	5.8 (3.9)	4.2 (2.7)	$F = 9.0, 29$	<0.01
Letter fluency ('D' words in 1 min)	16.1 (4.3)$^{+,-}$	6.2 (4.3)	4.6 (2.9)	$F = 25.3, 31$	<0.01
Semantic fluency (animals in 1 min)	23.7 (3.9)$^{+,-}$	11.8 (6.7)	8.0 (4.2)	$F = 23.9, 31$	<0.01
Abbreviated Boston Naming Test (max = 15)	14.8 (0.4)$^{+}$	11.4 (3.4)	12.6 (3.0)	K = 8.8, 2	0.01
Calculations (max = 5)	4.8 (0.4)$^{+,-}$	3.6 (0.7)	3.0 (1.5)	K = 11.5, 2	<0.01
NPI composite (max = 60)*	NA	31.6 (14.1)	31.5 (11.6)	$t = 0.03, 24$	0.98
NPI frequency × severity (max = 144)	NC	48.2 (22.8)	39.7 (16.7)	$t = 1.1, 24$	0.29

Means with standard deviations in parentheses reported unless noted otherwise. For tests between three groups, the *P*-value column indicates the *P*-value of the overall test statistic (ANOVA/Kruskal-Wallis). Superscript symbols indicate *post hoc* comparisons in which the healthy control group performance was significantly better than *C9orf72* carriers (+) or non-carriers (−) at $P < 0.05$.

FTLD-CDR = Frontotemporal Lobar Degeneration-Clinical Dementia Rating scale; df = degrees of freedom; NA = not applicable; NC = not collected.

*NPI composite represents a sum of the frequency × severity of the following NPI subscale measures: apathy, disinhibition, eating, euphoria, and aberrant motor behaviour.

Results

Demographic and clinical features

A stronger family history of dementia (Goldman score) characterized *C9orf72*+ bvFTD (Table 1). *C9orf72*+ and *C9orf72*− bvFTD showed no significant differences in demographic, clinical, and neuropsychological variables. Predominant executive dysfunction emerged in both groups compared to controls.

Patients with bvFTD with and without *C9orf72* expansions show overlapping but distinct atrophy patterns

Consistent with previous studies (Boeve *et al.*, 2012; Irwin *et al.*, 2013; Mahoney *et al.*, 2012; Sha *et al.*, 2012; Whitwell *et al.*, 2012), *C9orf72*+ bvFTD showed atrophy in bilateral anterior cingulate, dorsolateral prefrontal, orbitofrontal, anterior and posterior insular, and lateral parietal cortices, and precuneus, striatum, and bilateral thalamus compared to controls (Fig. 1). *C9orf72*− bvFTD exhibited similar but more extensive bilateral atrophy in frontotemporal, insular, cingulate, and striatal regions, with less extensive thalamic atrophy compared with controls. Comparing the bvFTD groups to each other, *C9orf72*+ bvFTD showed greater atrophy in bilateral medial pulvinar thalamic nuclei, postcentral gyrus, precuneus, and lateral parietal cortex, whereas *C9orf72*− bvFTD showed greater atrophy in bilateral anterior cingulate cortex, medial superior frontal gyri, and anterior insulae and left striatum (Supplementary Fig. 1).

Patients with bvFTD with and without *C9orf72* expansions feature topographically similar connectivity disruptions in the salience and sensorimotor networks

In the salience network, patient groups demonstrated similar connectivity reductions in bilateral anterior cingulate, medial superior frontal gyri, anterior insulae, and thalami compared to controls (Fig. 2A). No salience network connectivity differences emerged in the head-to-head patient group comparison.

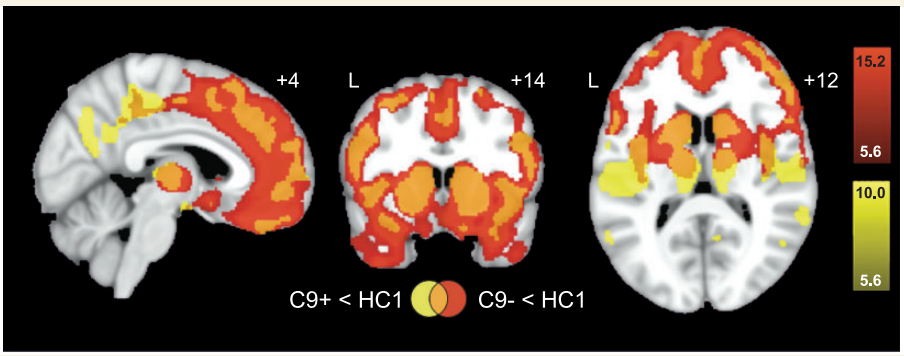

Figure 1 Atrophy patterns in bvFTD with and without *C9orf72* expansion. Fourteen *C9orf72* expansion carriers with bvFTD (five with comorbid MND) exhibit overlapping yet distinct atrophy patterns compared to 14 non-carriers matched for clinical syndrome. Group difference maps derived using voxel-based morphometry illustrate atrophy in *C9orf72* + bvFTD (yellow) and *C9orf72* − bvFTD (red) relative to healthy control group 1 (HC1). Groups showed overlapping atrophy (orange) in: bilateral pre- and subgenual anterior cingulate cortex, midcingulate cortex, dorsolateral prefrontal cortex, medial orbitofrontal cortex, anterior and posterior insula, striatum, and dorsomedial nucleus of thalamus. *C9orf72* + bvFTD showed atrophy in bilateral medial pulvinar nucleus and parietal cortex (not affected in *C9orf72* − bvFTD), whereas *C9orf72* − bvFTD showed more extensive atrophy in most typical bvFTD-affected regions. Significant clusters were defined at a *t*-threshold corrected for family-wise error of $P < 0.05$ with a minimum cluster size of 50 voxels. Colour bars represent *t*-scores, and statistical maps are superimposed on the Montreal Neurological Institute template brain. The left side of the axial and coronal images corresponds to the left (L) side of the brain. C9 + = *C9orf72* expansion carriers; C9 − = non-carriers for *C9orf72* expansion.

Adjusting the salience network analyses for atrophy had little influence on the patient versus control comparisons (Supplementary Table 2).

For the SMN, patient groups showed reduced connectivity in bilateral precentral and postcentral gyri and dorsal mid and posterior insulae compared to controls (Fig. 2A). Compared to *C9orf72* − bvFTD, *C9orf72* + bvFTD had reduced SMN connectivity in bilateral striatum and anterior thalami (Fig. 2B) that was due to connectivity reduction in *C9orf72* + and mild enhancement in *C9orf72* − (versus controls). No regions showed greater SMN connectivity in *C9orf72* + versus *C9orf72* − bvFTD. Atrophy-adjusted SMN findings were congruent with the unadjusted results (Supplementary Table 2).

Removing two patients with high movement from each group produced similar salience network and SMN findings (Supplementary Fig. 2).

Patients with bvFTD with and without *C9orf72* expansions exhibit divergent connectivity disruptions in the default mode network

Whereas *C9orf72* − bvFTD showed both enhanced (bilateral precuneus and right posterior cingulate cortex) and reduced (bilateral striatum, thalamus, midbrain and pons) DMN connectivity, *C9orf72* + bvFTD showed no connectivity differences compared to controls (Fig. 2A). Head-to-head patient group comparisons showed greater DMN connectivity in bilateral precuneus and right posterior cingulate cortex in *C9orf72* − bvFTD (Fig. 2B), reflecting DMN enhancements in *C9orf72* − bvFTD compared to controls (Fig. 2C). Atrophy-adjusted DMN maps produced topographically similar comparisons between *C9orf72* − bvFTD and controls and between bvFTD groups (Supplementary Table 2).

Removing two patients with high movement from each group produced new DMN decreases (midbrain, pons) and an increase (left angular gyrus) in *C9orf72* + bvFTD versus controls (Supplementary Fig. 2A); *C9orf72* − bvFTD DMN findings (Supplementary Fig. 2) resembled the original results (Fig. 2).

Behavioural symptom severity correlates with divergent network connectivity changes in salience and default mode networks

To examine the relationship between ICN strength and behavioural symptom severity, we correlated an NPI composite score with salience network and DMN connectivity in 26 patients (13 *C9orf72* +, 13 *C9orf72* −) for whom the NPI was available. Patients with more severe behavioural impairment showed lower connectivity between the right frontoinsular cortex seed and the left frontoinsula (Fig. 3, top panel). Adjusting for atrophy showed similar results with additional clusters emerging in left anterior midcingulate and right medial pulvinar nucleus in which lower connectivity predicted more severe behavioural symptoms, and a left anterior cingulate/medial prefrontal cluster in which greater connectivity predicted more severe behavioural symptoms (Supplementary Table 3), in keeping with one previous report (Farb *et al.*, 2013).

In the DMN, stronger connectivity between the right angular gyrus seed and bilateral angular gyri was associated with more severe behavioural symptoms (Fig. 3, bottom panel). With atrophy adjustment, bilateral posterior cingulate cortex, precuneus and left superior frontal gyri also showed greater DMN

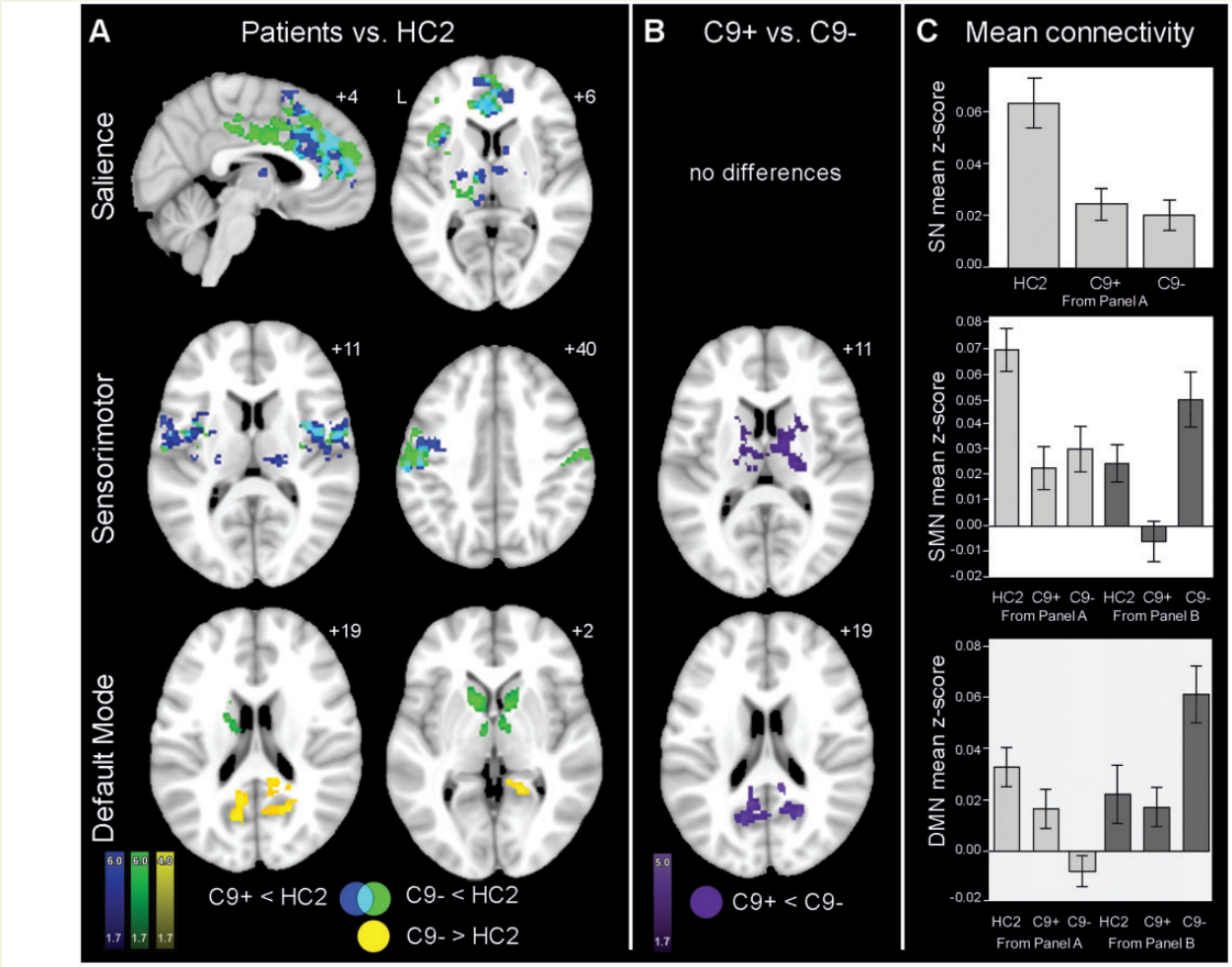

Figure 2 Intrinsic connectivity networks in bvFTD with and without *C9orf72* expansion. (**A**) Group difference task-free functional MRI maps reveal seed-based ICN reductions in *C9orf72* + bvFTD (dark blue) and *C9orf72* − bvFTD (green) relative to healthy control group 2 (HC2) for the three networks. Overlapping reductions are depicted in light blue. Whereas *C9orf72* + and *C9orf72* − bvFTD showed similar salience network and SMN connectivity reductions, only *C9orf72* − bvFTD showed DMN enhancements relative to HC2 (orange). (**B**) Head-to-head patient group comparisons showed no differences in the salience network but reduced relative SMN and DMN connectivity in *C9orf72* + bvFTD; no relative increases in SMN or DMN connectivity occurred in *C9orf72* + bvFTD. (**C**) Bar graphs illustrate mean intrinsic connectivity *z*-scores for HC2, *C9orf72* + bvFTD, and *C9orf72* − bvFTD for the salience network, SMN, and DMN. For the salience network, mean connectivity *z*-scores were derived within the union map of regions present in the *C9orf72* + bvFTD < HC2 and *C9orf72* − bvFTD < HC2 contrasts in **A** and show similar levels of salience network connectivity reduction in both groups. For the SMN, mean connectivity *z*-scores were derived within the union map of regions present in the *C9orf72* + bvFTD < HC2 and *C9orf72* − bvFTD < HC2 contrasts in **A** (light grey bars) and mean connectivity *z*-scores were derived from the *C9orf72* + bvFTD < *C9orf72* − bvFTD contrast in **B** (dark grey bars). For the DMN, mean connectivity *z*-scores were derived from the *C9orf72* − bvFTD < HC2 contrast in **A** (light grey bars) and mean connectivity *z*-scores were derived from the *C9orf72* + bvFTD < *C9orf72* − bvFTD contrast in **B** (dark grey bars). Error bars represent 1 SEM. Results in **A** and **B** are displayed at a joint cluster and extent probability threshold of $P < 0.05$, corrected at the whole-brain level. Statistical maps are superimposed on the Montreal Neurological Institute template brain. The left (L) side of the axial images corresponds to the left side of the brain. C9 + = *C9orf72* expansion carriers; C9 − = non-carriers for *C9orf72* expansion; HC2 = healthy control group 2; SN = salience network.

connectivity with worsening symptom severity (Supplementary Table 3).

When we compared *C9orf72* + and *C9orf72* − bvFTD for regions with differing correlations between NPI and grey matter atrophy, no significant clusters emerged at a family-wise error-corrected $P < 0.05$ (for $P < 0.001$ uncorrected results, see Supplementary material).

Role of medial pulvinar thalamus in *C9orf72*-related salience network disruption

BvFTD studies performed before identification of the *C9orf72* expansion identified the salience network as the primary network

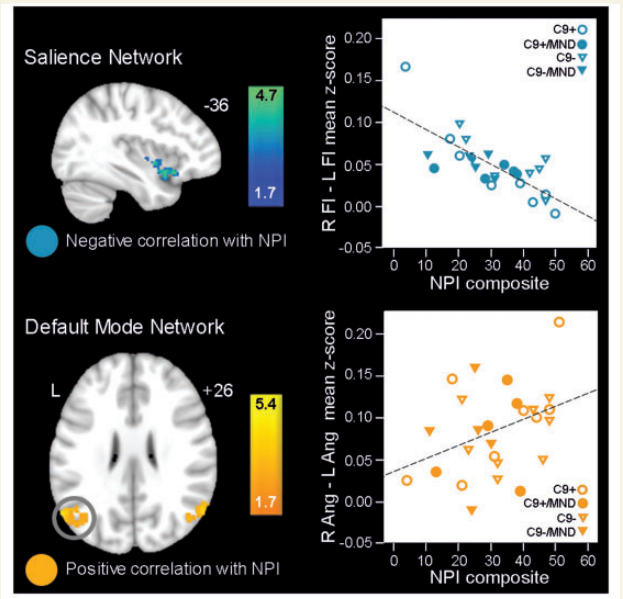

Figure 3 Symptom severity correlates with intrinsic connectivity network changes in bvFTD. NPI composite score correlated with salience network (*top*) and DMN (*bottom*) connectivity in 26 patients (13 *C9orf72* +, 13 *C9orf72* −) with bvFTD (10 with MND, five in each patient group). *Top panel*, *left*: For the salience network, weaker connectivity between the right frontoinsula seed and the left frontoinsula (blue) predicted greater behavioural symptom severity. *Bottom panel*, *left*: For the DMN, higher connectivity between the right angular gyrus and bilateral parietal regions was associated with worsening symptoms. Results are displayed at a joint cluster and extent probability threshold of $P < 0.05$, corrected at the whole-brain level. After identifying significant clusters, we plotted salience network mean connectivity scores (right frontoinsula (FI) seed to significant left frontoinsula cluster, *top panel*, *right*) and DMN mean connectivity scores (right angular (R Ang) gyrus seed to significant left angular gyrus cluster, *bottom panel*, *right*) versus the NPI composite scores, for visualization purposes only. Plots show mean connectivity *z*-scores within regions identified in the regression analyses for *C9orf72* + bvFTD (circle), *C9orf72* + bvFTD-MND (filled circle), *C9orf72* − bvFTD (triangle), *C9orf72* − bvFTD-MND (filled triangle) (right). Colour bars represent *t*-scores. All statistical maps are superimposed on the Montreal Neurological Institute template brain. The left side of the axial image corresponds to the left side of the brain. L = left; R = right.

target (Seeley *et al.*, 2009; Zhou *et al.*, 2010). In the present study, we found comparable salience network disruption in bvFTD regardless of *C9orf72* status. This result might seem surprising, considering that *C9orf72* + patients showed less severe atrophy within bvFTD-typical salience network 'epicentres' such as the anterior cingulate cortex and frontoinsula (Zhou *et al.*, 2012). Seeking to reconcile this apparent discordance, we reasoned that salience network connectivity disruption in *C9orf72* + bvFTD could be driven by a region of focal, strategic atrophy in *C9orf72* + bvFTD. Because this and previous *C9orf72* + bvFTD analyses found thalamic atrophy (Irwin *et al.*, 2013; Mahoney *et al.*, 2012; Sha *et al.*, 2012), we hypothesized that strategic thalamic degeneration might undermine salience network connectivity given the important role of the thalamus within all cortico-striato-thalamic networks (Parent and Hazrati, 1995).

To identify the specific thalamic subnucleus associated with salience network disruption, we performed a voxelwise analysis relating mean salience network connectivity scores to thalamic grey matter volume in *C9orf72* + bvFTD, which showed that left medial pulvinar nucleus atrophy predicted more severe salience network connectivity disruption (Fig. 4A). Although this finding should be interpreted with caution, it suggests that strategic thalamic degeneration may contribute to salience network disruption. To further pursue this possibility, we used the identified left medial pulvinar thalamus cluster (Fig. 4A) to seed an additional intrinsic connectivity analysis. This approach revealed that *C9orf72* + bvFTD showed significantly lower connectivity between left medial pulvinar thalamus and key salience network hubs in the anterior cingulate and insular cortices compared to *C9orf72* − bvFTD (Fig. 4B). A more relaxed statistical threshold ($t > 2.0$) revealed a second cluster in the right medial pulvinar (data not shown). Expanding the search volume to include the whole brain, we found that reduced salience network connectivity disruption also correlated with atrophy in parietal cortex and cerebellum but not with atrophy in typical bvFTD foci such as anterior insula or anterior cingulate. For *C9orf72* − bvFTD, atrophy within bilateral mediodorsal thalamic nuclei and typical bvFTD foci (right anterior insula, bilateral anterior cingulate) predicted more severe salience network connectivity disruption (data not shown).

Single-patient analyses detect network dysfunction in *C9orf72* expansion carriers with early-stage and slowly progressive bvFTD

We performed single-patient ICN analyses in two *C9orf72* carriers with prodromal bvFTD (Patients 1 and 2) and two with slowly progressive bvFTD (Patients 3 and 4) to characterize ICN alterations in patients with mild or undetectable atrophy (see Supplementary material for patient vignettes).

Patient 1, a female in her early fifties, had a history of mania and was diagnosed with non-amnestic mild cognitive impairment (FTLD-CDR 0.5). Voxel-based morphometry showed atrophy in the left ventrolateral thalamus (Supplementary Table 4). Reduced salience network connectivity emerged in bilateral anterior cingulate, medial superior frontal gyri, and cerebellum. She had SMN reductions in bilateral caudate. DMN enhancements in left dorsolateral prefrontal cortex, left anterior thalamus and left cerebellum emerged, with no DMN connectivity reductions (Fig. 5).

Patient 2 was clinically diagnosed with bvFTD during his fifties (FTLD-CDR 0.5), but he lacked some Neary bvFTD criteria (emotional blunting and loss of insight) and manifested only two of six core features (i.e. disinhibition and executive deficits) for possible bvFTD FTDC criteria. Voxel-based morphometry showed no significant differences compared with controls. Salience network reductions were observed in right medial superior frontal gyrus and

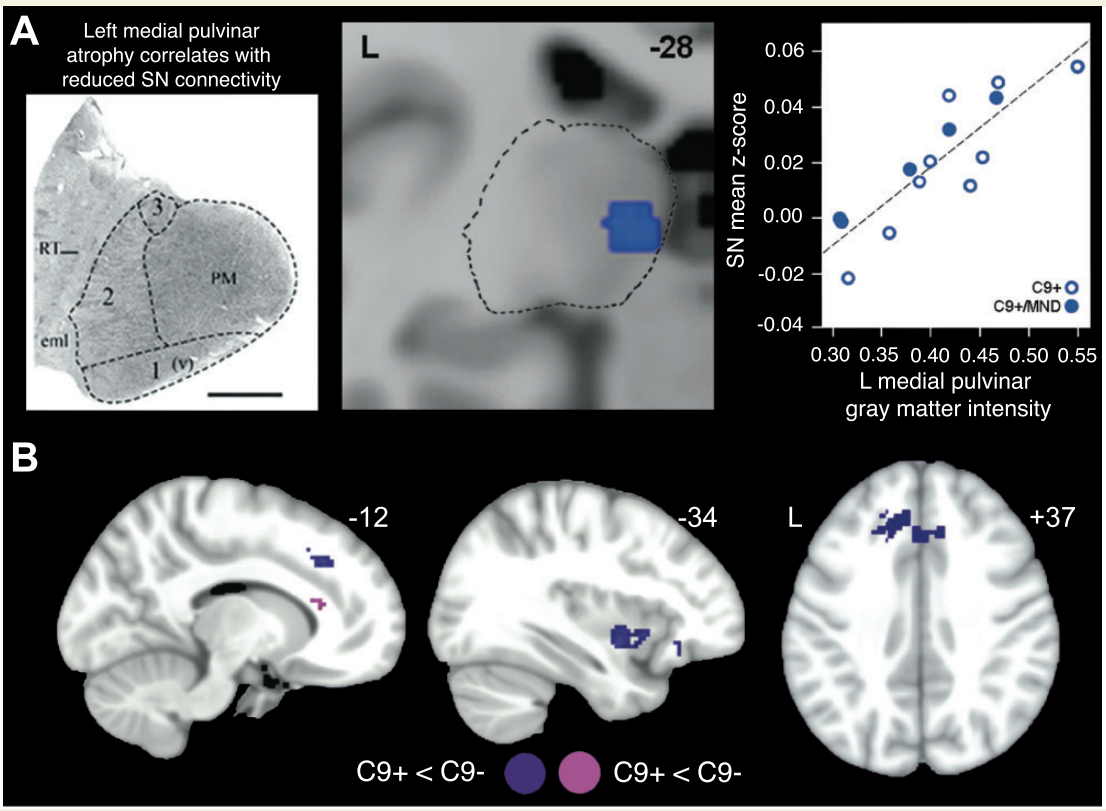

Figure 4 Abnormalities in medial pulvinar thalamus are associated with salience network disruption in *C9orf72*+ bvFTD. (**A**) In *C9orf72*+ bvFTD, lower mean salience network connectivity was associated with more severe left medial pulvinar thalamic atrophy (cluster shown at centre, data from cluster plotted at right). Results are displayed at a cluster threshold of $P < 0.01$ uncorrected ($t = 2.8$) with a minimum cluster size of 50 voxels. Cytoarchitecture of the medial pulvinar nucleus is shown for comparison (*left*, figure reproduced from Byne *et al*., 2007 with permission). (**B**) Group difference task-free functional MRI maps comparing *C9orf72*+ and *C9orf72*− bvFTD reveal ICN alterations to the left medial pulvinar region found in **A**. *C9orf72*+ bvFTD shows connectivity reductions to the left medial pulvinar in key salience network foci, including left ventral anterior insula and right anterior midcingulate cortex. Results are displayed at a joint cluster and extent probability threshold of $P < 0.05$, corrected at the whole brain level. Statistical maps are superimposed on the Montreal Neurological Institute template brain. Colour bars represent *t*-scores. The left side of the axial image corresponds to the left side of the brain. C9+ = *C9orf72* expansion carriers with bvFTD; C9+/MND = *C9orf72* expansion carriers with bvFTD-MND; C9− = non-carrier for *C9orf72* expansion with bvFTD; C9−/MND = non-carrier for *C9orf72* expansion with bvFTD-MND; eml = extra medullary lamina; L = left; PM = medial pulvinar; RT = reticular nucleus; SN = salience network; 1(v) = ventral pulvinar nucleus; 2 and 3 = lateral pulvinar nucleus.

anterior cingulate, right dorsolateral prefrontal cortex, bilateral thalamus, dorsal midbrain, pons and right cerebellum. SMN connectivity was reduced in the right cerebellum. DMN connectivity reductions were seen in the left putamen and connectivity enhancements emerged at the border between the left angular and middle occipital gyri (Fig. 5).

Building on previous work describing a 'bvFTD phenocopy' syndrome (Kipps *et al*., 2007, 2009, 2010; Hornberger *et al*., 2009), we recently reported four patients who met possible or probable bvFTD FTDC research criteria but were deemed 'slowly progressive' due to indolent progression and a normal structural MRI (Khan *et al*., 2012). Two of four patients harboured the *C9orf72* expansion; these patients (Patients 3 and 4 in the present study) met only possible bvFTD FTDC criteria due to a lack of characteristic atrophy on structural MRI.

Patient 3 was a 48-year-old male with slowly progressive bvFTD (FTLD-CDR 1; 'Patient 1' in Khan *et al*., 2012). Voxel-based morphometry showed no significant differences compared with controls. Salience network connectivity reductions in bilateral anterior cingulate, bilateral fronto-insulae, bilateral thalamus, dorsal midbrain, pons and bilateral cerebellum were detected (Fig. 5). SMN connectivity reduction involved the right putamen. The DMN showed enhancements in bilateral dorsolateral prefrontal cortex, left lateral parietal cortex, right precuneus, and right cerebellum (Fig. 5).

Patient 4 was a 48-year-old female with slowly progressive bvFTD (FTLD-CDR 1; 'Patient 2' in Khan *et al*., 2012). Voxel-based morphometry showed no significant differences compared with controls. No salience network disruptions were identified. The SMN showed enhancements in bilateral supplementary motor area, left striatum, left mediodorsal thalamic nucleus, dorsal midbrain, vermis and bilateral cerebellum. Enhanced DMN connectivity emerged in bilateral parieto-occipital cortex, left thalamus, midbrain tectum, pons, and vermis (Fig. 5).

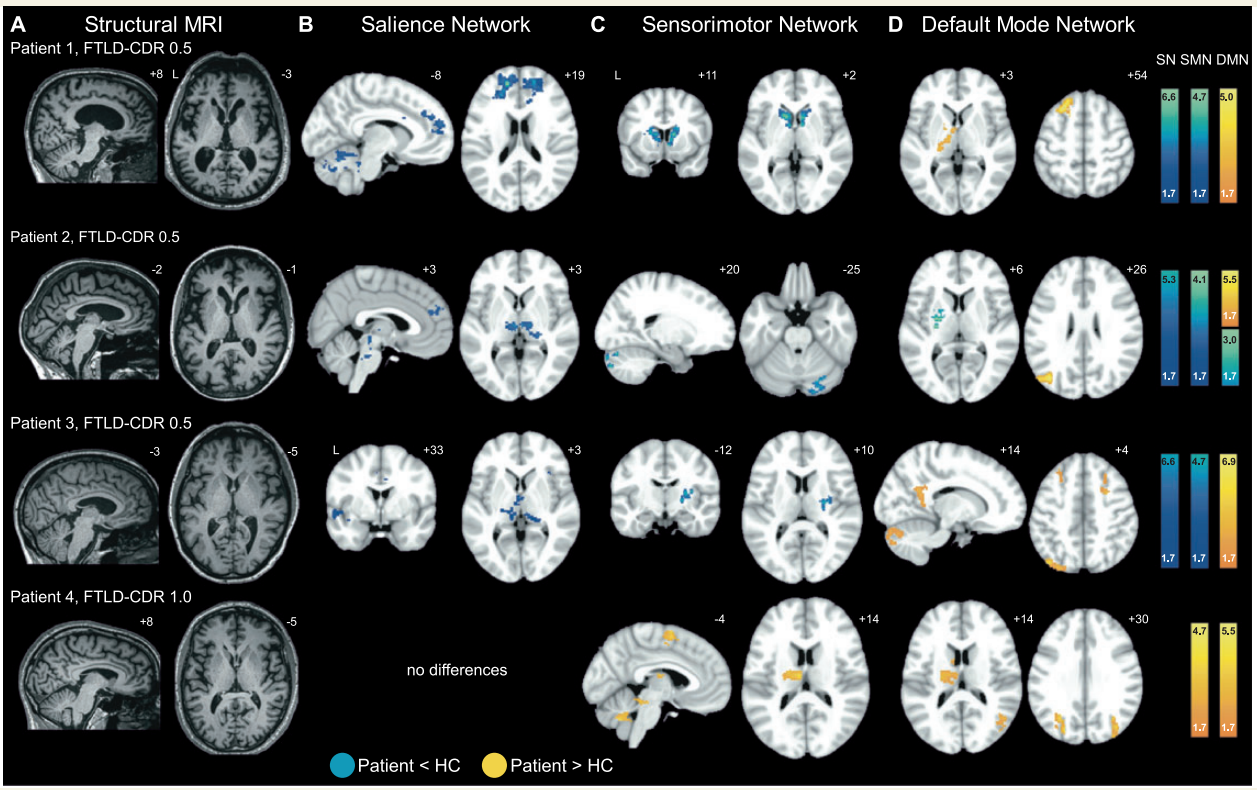

Figure 5 Single-patient analyses detect intrinsic connectivity network dysfunction in four *C9orf72* carriers with early-stage and slowly progressive disease. (**A**) Structural T_1-weighted brain MRI with FTLD-CDR scale total score. (**B**) Salience network, (**C**) SMN, and (**D**) DMN contrast maps comparing each patient to 30 healthy controls matched to that patient are thresholded at a joint cluster and extent probability threshold of $P < 0.05$, corrected at the whole brain level. Despite mild or absent brain atrophy, most patients showed salience network and SMN reductions (blue) and DMN enhancements (orange). Statistical maps are superimposed on the Montreal Neurological Institute template brain. Colour bars represent *t*-scores. The left (L) side of the axial and coronal images corresponds to the left side of the brain. HC = healthy control participants; SN = salience network.

In summary, three of four *C9orf72* carriers with prodromal or slowly progressive bvFTD exhibited single-subject level salience network connectivity reductions, including medial thalamus in Patients 2 and 3; none had salience network connectivity increases. SMN findings were mixed in these patients, who lacked clinical MND. All four single-patient analyses showed DMN enhancements (Fig. 5).

Discussion

Patients with bvFTD are united by a core behavioural symptom profile but represent a heterogeneous spectrum of underlying pathobiology. Collapsing these diverse patients into a single group, previous studies have shown that bvFTD is associated with salience network atrophy (Seeley *et al.*, 2009) accompanied by reduced salience network connectivity and increased DMN connectivity (Zhou *et al.*, 2010; Whitwell *et al.*, 2011; Farb *et al.*, 2013), both of which correlate with clinical severity (Zhou *et al.*, 2010; Farb *et al.*, 2013). Our key finding is that we demonstrated how patients with bvFTD due to the *C9orf72* expansion show a similar pattern of network dysfunction despite contrasting atrophy patterns compared with sporadic bvFTD (Boeve *et al.*, 2012; Irwin *et al.*, 2013; Sha *et al.*, 2012; Whitwell *et al.*, 2012). We added the SMN, not previously examined in FTD, due to the close link between bvFTD and MND. Our findings show that *C9orf72*+ and *C9orf72*− bvFTD are accompanied by topographically similar salience network and SMN connectivity reductions, suggesting that ICN measures mirrored the clinical syndrome. Although *C9orf72*− bvFTD showed DMN enhancements, replicating previous work (Zhou *et al.*, 2010; Whitwell *et al.*, 2011; Farb *et al.*, 2013), patients with full-blown *C9orf72*+ bvFTD showed no such enhancements. Seeking to determine how *C9orf72*+ and *C9orf72*− bvFTD produce comparable salience network disruption despite contrasting atrophy patterns, we found a novel link between focal, strategic atrophy of the medial pulvinar nucleus of the thalamus and overall salience network disruption in *C9orf72*+ bvFTD. We propose that this strategic thalamic lesion aids in generating full-blown bvFTD in patients who lack severe atrophy in core bvFTD structures. At the single-subject level, patients with prodromal and slowly progressive *C9orf72*+ bvFTD showed a consistent pattern of salience network and SMN disruption alongside heightened DMN connectivity, suggesting that eventual *C9orf72*-associated spread into posterior cortices may quell DMN hyperconnectivity present in earlier stages. Overall, the findings illustrate (i) how contrasting regional atrophy patterns can converge on a unifying syndromic

pattern of network dysfunction; and (ii) that task-free functional MRI holds promise for detecting prodromal disease in genetic FTD.

Intrinsic connectivity network disruption reconciles distinct atrophy patterns observed in *C9orf72* carriers and non-carriers

Sporadic bvFTD features early (Seeley *et al*., 2008) and consistent damage to the anterior insula, anterior cingulate, and orbitofrontal cortices (Boccardi *et al*., 2005; Schroeter *et al*., 2007), which represent key salience network regions. Although *C9orf72* + and *C9orf72* − bvFTD showed overlapping atrophy in these regions, *C9orf72* + patients have less severe atrophy in these areas and greater involvement of medial pulvinar thalamus and parietal cortex. These findings suggest that either mild degeneration in bvFTD 'epicentres' or degeneration in less typical regions is sufficient to produce the *C9orf72* + bvFTD clinical syndrome. Matching *C9orf72* + and *C9orf72* − groups for clinical severity and syndrome, we hypothesized that task-free functional MRI would detect convergent ICN alterations. As predicted, we found salience network connectivity reductions of a similar magnitude and topography in *C9orf72* + and *C9orf72* − bvFTD, suggesting that the salience network alterations, rather than atrophy, parallel clinical syndrome. Moreover, greater salience network impairment correlated with more severe behavioural symptoms in both groups, further illustrating the clinical relevance of salience network integrity (Zhou *et al*., 2010; Farb *et al*., 2013).

Although previous studies have identified thalamic atrophy as characteristic of *C9orf72* carriers (Irwin *et al*., 2013; Mahoney *et al*., 2012; Sha *et al*., 2012), little attention has been paid to the precise topography of thalamic involvement, a critical issue considering the diverse and specialized functions and connections contained within neighbouring subnuclei. Although both patient groups showed thalamic atrophy relative to controls, atrophy in the bilateral medial pulvinar nuclei was seen only in *C9orf72* + bvFTD compared to controls. Searching across the entire thalamus, we found that medial pulvinar atrophy (left > right in this sample) predicted reduced salience network connectivity in *C9orf72* + bvFTD only, and that *C9orf72* + bvFTD shows significantly more impaired left medial pulvinar connectivity to key salience network epicentres compared with *C9orf72* − bvFTD. These findings suggest a key role for medial pulvinar thalamus in mediating salience network disruption in *C9orf72* + bvFTD.

In contrast to the lateral and inferior pulvinar, whose projections target striate and extrastriate cortex (Robinson and Petersen, 1992; Yeterian and Pandya, 1995), the medial pulvinar has prominent reciprocal connections with orbitofrontal, parahippocampal, cingulate, insular and amygdalar regions (Jones and Burton, 1976; Mufson and Mesulam, 1984; Romanski *et al*., 1997), major nodes of the human salience network (Seeley *et al*., 2007). Primate electrophysiological studies suggest that the lateral and inferior pulvinar primarily respond to simple visual stimuli, whereas the medial pulvinar appears to evaluate the salience of visual stimuli (Robinson, 1993).

Could medial pulvinar dysfunction contribute to psychosis in *C9orf72* + bvFTD? Patients with schizophrenia show reduced right medial pulvinar volume, neuron number (Byne *et al*., 2007), and D2/D3 receptor binding (Yasuno *et al*., 2004; Buchsbaum *et al*., 2006), suggesting a potential basis for the higher incidence of psychosis in *C9orf72* + bvFTD (Boeve *et al*., 2012; Simón-Sánchez *et al*., 2012; Snowden *et al*., 2012). In the present study, 2 of 14 patients with *C9orf72* + bvFTD showed signs of psychosis. Although our patient groups showed a similar frequency of psychotic symptoms, future studies may help to determine whether medial pulvinar degeneration predisposes to psychosis in *C9orf72* + bvFTD.

Previous bvFTD intrinsic connectivity studies have focused on the salience and default mode networks, but the close relationship between bvFTD and MND compelled us to investigate the SMN, which overlaps with the corticospinal motor system and shows abnormal connectivity in ALS (Mohammadi *et al*., 2009; Douaud *et al*., 2011; Tedeschi *et al*., 2012). We found that both patient groups had SMN reductions in bilateral primary motor cortices. Compared to *C9orf72* − bvFTD, *C9orf72* + patients showed greater SMN disruption, perhaps because *C9orf72* + bvFTD poses greater risk for subclinical motor system degeneration than does sporadic bvFTD. Longitudinal studies are needed to determine whether SMN alterations predict future clinical motor system deficits.

The DMN was first identified based on its deactivation in response to diverse cognitive and behavioural tasks, many of which recruit the salience network and other networks (Raichle *et al*., 2001). More recent work has shown that the DMN consists of anatomically and functionally distinct subnetworks. A posterior DMN comprised of the angular gyrus, posterior cingulate cortex, and precuneus appears critical for episodic retrieval functions, whereas an anterior DMN anchored by the medial prefrontal cortex supports meta-cognitive functions impaired in bvFTD, such as theory of mind and self-reflection (Spreng and Grady, 2010; Sestieri *et al*., 2011; Mars, 2012). DMN findings to date in bvFTD generally support this functional-anatomical segregation, with most studies showing reduced connectivity within anterior but increased connectivity within posterior DMN nodes (Zhou *et al*., 2010; Whitwell *et al*., 2011; Farb *et al*., 2013), although one study reported DMN increases only (Borroni *et al*., 2012) and another failed to demonstrate DMN alterations (Filippi *et al*., 2013). Our findings suggest that group analyses may yield heterogeneous results because DMN connectivity may depend on the patient's disease stage and whether bvFTD is due to *C9orf72*. DMN enhancements may occur early in *C9orf72* + bvFTD but attenuate as disease spreads more posteriorly. In contrast, when the posterior DMN remains intact, as in most patients with *C9orf72* − bvFTD, DMN connectivity intensifies as clinical status and salience network integrity decline.

Single-subject imaging metrics for early-stage bvFTD: proof of concept

C9orf72 carriers with early-stage or slowly progressive bvFTD may show little or no atrophy on routine structural MRI (Boeve

et al., 2012; Khan *et al*., 2012) despite major clinical impairment, suggesting that neural dysfunction, rather than neuronal and synaptic loss, must account for the clinical syndrome. To explore this idea, we performed single-patient analyses in four *C9orf72* carriers: one with behavioural-executive mild cognitive impairment, one with behavioural symptoms not meeting bvFTD criteria, and two with slowly progressive bvFTD. The single patient analyses were consistent with the group ICN results, with three of four patients showing salience network reductions; all had DMN enhancements. Two patients, including one with a structurally normal MRI, showed prominent medial pulvinar thalamic disconnection from the salience network, suggesting that for some patients with the *C9orf72* expansion, early thalamic dysfunction and disconnection may be the primary or even sole driver of salience network functional breakdown. This possibility evokes a neglected literature on 'thalamic dementia,' historically ascribed to a range of aetiologies. Although many patients in this literature suffered from vascular lesions (Schmahmann, 2003; Carrera and Bogousslavsky, 2006) or prion disease (Petersen *et al*., 1992; Kornfeld and Seelinger, 1994), others showed either no clear neuropathology or ubiquitin-only immunoreactive inclusions, at times associated with clinical and pathological MND (Kosaka and Mehraein, 1978; Deymeer *et al*., 1989; Radanovic *et al*., 2003). Based on the present findings, we speculate that *C9orf72* accounts for most non-vascular, non-prion thalamic dementia in the literature. Most importantly, our single patient studies suggest that bvFTD-related network dysfunction emerges early, may explain clinical deficits, and can be detected with task-free functional MRI, justifying further studies of this modality for early diagnosis in inherited and sporadic FTD.

Limitations and future studies

A limitation of this study was the relatively small group of *C9orf72* carriers, which may have limited power to detect subtle effects and required us to combine participants imaged on two MRI scanners whose platforms have not been formally standardized. To minimize the impact of this approach, we balanced groups for scanner and controlled for scanner in all analyses, but the present findings should be interpreted with caution until replicated in larger numbers on a single MRI scanner. *C9orf72* carriers present with heterogeneous syndromes, even within families. Thus, group results may not generalize to all patients, but we found that single-patient ICN analyses had the power to detect distinct patterns of altered connectivity consistent with group-level *C9orf72*+ bvFTD analyses, even in prodromal and slowly progressive disease. Single patient analyses represent an important step toward understanding rare genetic disorders for which it may take years to assemble a sufficient sample for group analyses. Standardization of single-subject task-free functional MRI analyses will be needed prior to clinical use, but our preliminary results build a foundation for within-subject longitudinal analyses geared toward understanding the natural history of bvFTD and monitoring disease status in response to treatment.

Acknowledgements

We thank Dr. Catherine Lomen-Hoerth for performing EMGs on participants. We also thank our participants and their families for their valuable contributions to research.

Funding

National Institute on Aging (NIA grant number K23 AG039414 to S.E.L., NIH-NIA Diversity Supplement to P50 AG023501 to J.S.Y., RC1 AG035610 to G.C., R01 AG026938 to D.H.G., R01 AG031278 and R01 AG038791 to A.L.B., R01 AG032289 to J.H.K., R01 AG032306 to H.J.R., P50 AG023501 to B.L.M. and W.W.S., and P01 AG019724 to M.W.W., B.L.M., and W.W.S.); the National Institute of Neurological Disorders and Stroke (NINDS grant number T32 NS048004-07 to M.P., and R01 NS080882 to R.R.); the Larry L. Hillblom Foundation (grant number 2012-A-015-FEL to J.S.Y., and 2007/2I to B.L.M.); the Bluefield Project to Cure FTD, Association for FTD, Alzheimer's Drug Discovery Foundation to A.L.B., and the Tau Consortium to G.C., D.H.G., A.L.B.

Supplementary material

Supplementary material is available at *Brain* online.

References

Biswal B, Yetkin FZ, Haughton VM, Hyde JS. Functional connectivity in the motor cortex of resting human brain using echo-planar MRI. Magn Reson Med 1995; 34: 537–41.

Boccardi M, Sabattoli F, Laakso MP, Testa C, Rossi R, Beltramello A, et al. Frontotemporal dementia as a neural system disease. Neurobiol Aging 2005; 26: 37–44.

Boeve BF, Boylan KB, Graff-Radford NR, DeJesus-Hernandez M, Knopman DS, Pedraza O, et al. Characterization of frontotemporal dementia and/or amyotrophic lateral sclerosis associated with the GGGGCC repeat expansion in C9ORF72. Brain 2012; 135: 765–83.

Borroni B, Alberici A, Cercignani M, Premi E, Serra L, Cerini C, et al. Granulin mutation drives brain damage and reorganization from preclinical to symptomatic FTLD. Neurobiol Aging 2012; 33: 2506–20.

Boxer AL, Mackenzie IR, Boeve BF, Baker M, Seeley WW, Crook R, et al. Clinical, neuroimaging and neuropathological features of a new chromosome 9p-linked FTD-ALS family. J Neurol Neurosurg Psychiatry 2011; 82: 196–203.

Brett M, Anton J-L, Valabregue R, Poline J-B. Region of interest analysis using an SPM toolbox [abstract]. Presented at the 8th International Conference on Functional Mapping of the Human Brain, June 2-6, 2002, Sendai, Japan.

Brooks BR, Miller RG, Swash M, Munsat TL. World Federation of Neurology Research Group on Motor Neuron Diseases. El Escorial revisited: revised criteria for the diagnosis of amyotrophic lateral sclerosis. Amyotroph Lateral Scler Other Motor Neuron Disord 2000; 1: 293–9.

Buchsbaum MS, Christian BT, Lehrer D, Narayanan T, Shi B, Mantil J, et al. D2/D3 dopamine receptor binding with [F-18]fallypride in thalamus and cortex of patients with schizophrenia. Schizophr Res 2006; 85: 232–44.

Byne W, Fernandes J, Haroutunian V, Huacon D, Kidkardnee S, Kim J, et al. Reduction of right medial pulvinar volume and neuron number in schizophrenia. Schizophr Res 2007; 90: 71–5.

Carrera E, Bogousslavsky J. The thalamus and behavior: effects of anatomically distinct strokes. Neurology 2006; 66: 1817–1823.

Casanova R, Srikanth R, Baer A, Laurienti PJ, Burdette JH, Hayasaka S, et al. Biological parametric mapping: a statistical toolbox for multimodality brain image analysis. NeuroImage 2007; 34: 137–43.

Cummings JL, Mega M, Gray K, Rosenberg-Thompson S, Carusi DA, Gornbein J. The Neuropsychiatric Inventory: comprehensive assessment of psychopathology in dementia. Neurology 1994; 44: 2308–14.

DeJesus-Hernandez M, Mackenzie IR, Boeve BF, Boxer AL, Baker M, Rutherford NJ, et al. Expanded GGGGCC hexanucleotide repeat in noncoding region of C9ORF72 causes chromosome 9p-linked FTD and ALS. Neuron 2011; 72: 245–56.

Deymeer F, Smith TW, DeGirolami U, Drachman DA. Thalamic dementia and motor neuron disease. Neurology 1989; 39: 58–61.

Dopper EG, Rombouts SA, Jiskoot LC, Heijer Td, de Graaf JR, Koning Id, et al. Structural and functional brain connectivity in presymptomatic familial frontotemporal dementia. Neurology 2014; 83: e19–26.

Douaud G, Filippini N, Knight S, Talbot K, Turner MR. Integration of structural and functional magnetic resonance imaging in amyotrophic lateral sclerosis. Brain 2011; 134: 3470–9.

Farb NAS, Grady CL, Strother S, Tang-Wai DF, Masellis M, Black S, et al. Abnormal network connectivity in frontotemporal dementia: evidence for prefrontal isolation. Cortex 2013; 49: 1856–73.

Filippi M, Agosta F, Scola E, Canu E, Magnani G, Marcone A, et al. Functional network connectivity in the behavioral variant of frontotemporal dementia. Cortex 2013; 49: 2389–401.

Folstein MF, Robins LN, Helzer JE. The mini-mental state examination. Arch Gen Psychiatry 1983; 40: 812.

Gardner RC, Boxer AL, Trujillo A, Mirsky JB, Guo CC, Gennatas ED, et al. Intrinsic connectivity network disruption in progressive supranuclear palsy. Ann Neurol 2013; 73: 603–16.

Habas C, Kamdar N, Nguyen D, Prater K, Beckmann CF, Menon V, et al. Distinct cerebellar contributions to intrinsic connectivity networks. J Neurosci 2009; 29: 8586–94.

Hornberger M, Shelley BP, Kipps CM, Piguet O, Hodges JR. Can progressive and non-progressive behavioural variant frontotemporal dementia be distinguished at presentation? J Neurol Neurosurg Psychiatry 2009; 80: 591–3.

Irwin DJ, McMillan CT, Brettschneider J, Libon DJ, Powers J, Rascovsky K, et al. Cognitive decline and reduced survival in C9orf72 expansion frontotemporal degeneration and amyotrophic lateral sclerosis. J Neurol Neurosurg Psychiatry 2013; 84: 163–9.

Jones EG, Burton H. A projection from the medial pulvinar to the amygdala in primates. Brain Res 1976; 104: 142–7.

Khan BK, Yokoyama JS, Takada LT, Sha SJ, Rutherford NJ, Fong JC, et al. Atypical, slowly progressive behavioural variant frontotemporal dementia associated with C9ORF72 hexanucleotide expansion. J'Neurol Neurosurg Psychiatry 2012; 83: 358–64.

Kipps CM, Hodges JR, Fryer TD, Nestor PJ. Combined magnetic resonance imaging and positron emission tomography brain imaging in behavioural variant frontotemporal degeneration: refining the clinical phenotype. Brain 2009; 132: 2566–78.

Kipps CM, Hodges JR, Hornberger M. Nonprogressive behavioural frontotemporal dementia: recent developments and clinical implications of the 'bvFTD phenocopy syndrome'. Curr Opin Neurol 2010; 23: 628–32.

Kipps CM, Nestor PJ, Fryer TD, Hodges JR. Behavioural variant frontotemporal dementia: not all it seems? Neurocase 2007; 13: 237–47.

Knopman DS, Kramer JH, Boeve BF, Caselli RJ, Graff-Radford NR, Mendez MF, et al. Development of methodology for conducting clinical trials in frontotemporal lobar degeneration. Brain 2008; 131: 2957–68.

Kornfeld M, Seelinger DF. Pure thalamic dementia with a single focus of spongiform change in cerebral cortex. Clin Neuropathol 1994; 13: 77–81.

Kosaka K, Mehraein P. [Amyotrophic lateral sclerosis with degeneration of thalamus and substantia nigra (author's transl)]. Acta Neuropathol 1978; 44: 241–4.

Liu W, Miller BL, Kramer JH, Rankin K, Wyss-Coray C, Gearhart R, et al. Behavioral disorders in the frontal and temporal variants of frontotemporal dementia. Neurology 2004; 62: 742–8.

Mahoney CJ, Beck J, Rohrer JD, Lashley T, Mok K, Shakespeare T, et al. Frontotemporal dementia with the C9ORF72 hexanucleotide repeat expansion: clinical, neuroanatomical and neuropathological features. Brain 2012; 135: 736–50.

Mars RB. On the relationship between the "default mode network" and the "social brain". 2012; 6: 189.

Mohammadi B, Kollewe K, Samii A, Krampfl K, Dengler R, Münte TF. Changes of resting state brain networks in amyotrophic lateral sclerosis. Exp Neurol 2009; 217: 147–53.

Morris JC. The Clinical Dementia Rating (CDR): current version and scoring rules. Neurology 1993; 43: 2412–14.

Mufson EJ, Mesulam MM. Thalamic connections of the insula in the rhesus monkey and comments on the paralimbic connectivity of the medial pulvinar nucleus. J Comp Neurol 1984; 227: 109–20.

Neary D, Snowden JS, Gustafson L, Passant U, Stuss D, Black S, et al. Frontotemporal lobar degeneration: a consensus on clinical diagnostic criteria. Neurology 1998; 51: 1546–54.

Ofen N, Kao Y-C, Sokol-Hessner P, Kim H, Whitfield-Gabrieli S, Gabrieli JDE. Development of the declarative memory system in the human brain. Nat Neurosci 2007; 10: 1198–205.

Parent A, Hazrati LN. Functional anatomy of the basal ganglia. I. The cortico-basal ganglia-thalamo-cortical loop. Brain Res Brain Res Rev 1995; 20: 91–127.

Petersen RB, Tabaton M, Berg L, Schrank B, Torack RM, Leal S, et al. Analysis of the prion protein gene in thalamic dementia. Neurology 1992; 42: 1859.

Poline JB, Worsley KJ, Evans AC, Friston KJ. Combining spatial extent and peak intensity to test for activations in functional imaging. NeuroImage 1997; 5: 83–96.

Radanovic M, Rosemberg S, Adas R, Miranda SC, Caramelli P, Caixeta L, et al. Frontotemporal dementia with severe thalamic involvement: a clinical and neuropathological study. Arq Neuropsiquiatr 2003; 61: 930–5.

Raichle ME, MacLeod AM, Snyder AZ, Powers WJ, Gusnard DA, Shulman GL. A default mode of brain function. Proc Natl Acad Sci USA 2001; 98: 676–82.

Rascovsky K, Hodges JR, Knopman D, Mendez MF, Kramer JH, Neuhaus J, et al. Sensitivity of revised diagnostic criteria for the behavioural variant of frontotemporal dementia. Brain 2011; 134: 2456–77.

Renton AE, Majounie E, Waite A, Simón-Sánchez J, Rollinson S, Gibbs JR, et al. A hexanucleotide repeat expansion in C9ORF72 is the cause of chromosome 9p21-linked ALS-FTD. Neuron 2011; 72: 257–68.

Robinson DL. Functional contributions of the primate pulvinar. Prog Brain Res 1993; 95: 371–80.

Robinson DL, Petersen SE. The pulvinar and visual salience. Trends Neurosci 1992; 15: 127–32.

Romanski LM, Giguere M, Bates JF, Goldman-Rakic PS. Topographic organization of medial pulvinar connections with the prefrontal cortex in the rhesus monkey. J Comp Neurol 1997; 379: 313–32.

Schmahmann JD. Vascular syndromes of the thalamus. Stroke 2003; 34: 2264–78.

Schroeter ML, Raczka K, Neumann J, Yves von Cramon D. Towards a nosology for frontotemporal lobar degenerations-a meta-analysis involving 267 subjects. NeuroImage 2007; 36: 497–510.

Seeley WW, Crawford R, Rascovsky K, Kramer JH, Weiner M, Miller BL, et al. Frontal paralimbic network atrophy in very mild behavioral variant frontotemporal dementia. Arch Neurol 2008; 65: 249–55.

Seeley WW, Crawford RK, Zhou J, Miller BL, Greicius MD. Neurodegenerative diseases target large-scale human brain networks. Neuron 2009; 62: 42–52.

Seeley WW, Menon V, Schatzberg AF, Keller J, Glover GH, Kenna H, et al. Dissociable intrinsic connectivity networks for salience processing and executive control. J Neurosci 2007; 27: 2349–56.

Sestieri C, Corbetta M, Romani GL, Shulman GL. Episodic memory retrieval, parietal cortex, and the default mode network: functional and topographic analyses. J Neurosci 2011; 31: 4407–20.

Sha SJ, Takada LT, Rankin KP, Yokoyama JS, Rutherford NJ, Fong JC, et al. Frontotemporal dementia due to C9ORF72 mutations: clinical and imaging features. Neurology 2012; 79: 1002–11.

Simón-Sánchez J, Dopper EGP, Cohn-Hokke PE, Hukema RK, Nicolaou N, Seelaar H, et al. The clinical and pathological phenotype of C9orf72 hexanucleotide repeat expansions. Brain 2012; 135: 723–35.

Smith SM, Fox PT, Miller KL, Glahn DC, Fox PM, Mackay CE, et al. Correspondence of the brain's functional architecture during activation and rest. Proc Natl Acad Sci USA 2009; 106: 13040–5.

Snowden JS, Rollinson S, Thompson JC, Harris JM, Stopford CL, Richardson AMT, et al. Distinct clinical and pathological characteristics of frontotemporal dementia associated with C9ORF72 mutations. Brain 2012; 135: 693–708.

Spreng RN, Grady CL. Patterns of brain activity supporting autobiographical memory, prospection, and theory of mind, and their relationship to the default mode network. J Cogn Neurosci 2010; 22: 1112–3.

Tedeschi G, Trojsi F, Tessitore A, Corbo D, Sagnelli A, Paccone A, et al. Interaction between aging and neurodegeneration in amyotrophic lateral sclerosis. Neurobiol Aging 2012; 33: 886–98.

Van Dijk KRA, Sabuncu MR, Buckner RL. The influence of head motion on intrinsic functional connectivity MRI. NeuroImage 2012; 59: 431–8.

Whitwell JL, Josephs KA, Avula R, Tosakulwong N, Weigand SD, Senjem ML, et al. Altered functional connectivity in asymptomatic MAPT subjects: a comparison to bvFTD. Neurology 2011; 77: 866–74.

Whitwell JL, Weigand SD, Boeve BF, Senjem ML, Gunter JL, DeJesus-Hernandez M, et al. Neuroimaging signatures of frontotemporal dementia genetics: C9ORF72, tau, progranulin and sporadics. Brain 2012; 135: 794–806.

Yasuno F, Suhara T, Okubo Y, Sudo Y, Inoue M, Ichimiya T, et al. Low dopamine d(2) receptor binding in subregions of the thalamus in schizophrenia. Am J Psychiatry 2004; 161: 1016–22.

Yeterian EH, Pandya DN. Corticostriatal connections of extrastriate visual areas in rhesus monkeys. J Comp Neurol 1995; 352: 436–57.

Zhou J, Gennatas ED, Kramer JH, Miller BL, Seeley WW. Predicting regional neurodegeneration from the healthy brain functional connectome. Neuron 2012; 73: 1216–27.

Zhou J, Greicius MD, Gennatas ED, Growdon ME, Jang JY, Rabinovici GD, et al. Divergent network connectivity changes in behavioural variant frontotemporal dementia and Alzheimer's disease. Brain 2010; 133: 1352–67.

Zielinski BA, Gennatas ED, Zhou J, Seeley WW. Network-level structural covariance in the developing brain. Proc Natl Acad Sci USA 2010; 107: 18191–6.